

EFFECT OF VIBRATION IN COOLING CHANNEL ON HEAT TRANSFER OF AVIATION KEROSENE FLOWING UNDER DIFFERENT PRESSURES

by

**Yuxiang HAN^a, Mantang CHEN^b, Zilong PENG^a,
Zhixiong HAN^c, and Hao ZAN^{a*}**

^a Jiangsu University of Science and Technology, Jiangsu, China

^b Beijing Power Machinery Institute, Beijing, China

^c Harbin Institute of Technology, Heilongjiang, China

Original scientific paper

<https://doi.org/10.2298/TSCI220523114H>

In this study, experimental methods are used to investigate the effects of different vibration and pressure parameters on heat transfer performance are analyzed. The results show that at a subcritical pressure (0.1 MPa), the external vibration begins to affect the heat transfer when the fuel passes the phase-change point and becomes gaseous. At a near-critical pressure (3 MPa), the external vibration deteriorates the heat transfer of fuel across the critical-temperature zone. At the supercritical pressure (5 MPa), the external vibration intensifies the heat transfer in the hot end of the channel only when the fuel is below the critical temperature and the internal wall is above the critical pressure. Combined with data analysis, it can be seen that the external vibration mainly acts on the temperature boundary layer of the fuel oil to affect the wall temperature and heat transfer coefficient.

Key words: *scramjet engine, cooling channel, vibration, flow heat transfer*

Introduction

Hypersonic flight technology is a cutting-edge technology for the aerospace industry in the 21st century. An aspirated hypersonic vehicle is one that is operated by an aspirated scramjet engine and flies at a Mach number exceeding 5 [1-4]. However, the high Mach number of scramjet engines results in severe thermal protection problems. When they fly at Mach 6, the peak of the heat flow in the combustion chamber caused by aerodynamic heat and combustion heat release can reach up to 3 MW/m², and the temperature of the central flow in the combustion chamber reaching 2500-3000 K [5]. Regenerative cooling is regarded as one of the best cooling methods to avoid the mass penalty associated with the use of additional coolants [6]. Scramjet engines have a simple structure but impose severe limitations on structural mass. Therefore, they are manufactured using thin-walled structures that are subjected to significant aerodynamic and aerodynamic thermal loads. However, their wall plates may exhibit vibration problems under the action of supersonic air-flow. Many system factors affect the vibration characteristics of wall plates, such as the dynamic pressure of the airflow, angle of the incoming airflow, support form of the structure, compression force of the mid-plane, structural damping, and material properties [7, 8].

* Corresponding author, e-mail: zanhao870127@163.com

Wall vibration significantly affects the heat transfer characteristics of fluid-flow inside the tube. Prior to the 1960's, the vibration of tubes in heat exchangers as a destructive factor has been prevented. Since the 1960's, scholars have discovered that secondary flows will be induced when the vibration amplitude of tubes in a heat exchanger reaches a certain intensity, which will then increase the convective heat transfer coefficient. The convection of wall vibration has been investigated extensively despite the simple structure of mechanical vibration devices and the relative ease in adjusting the parameters, including the amplitude and frequency. As such, these devices are suitable for performing comprehensive investigations of the effect of vibration parameters on heat transfer. A group of scholars have systematically investigated the effect of vibration on heat transfer under natural convection and forced conditions, separately [9-26].

Table 1. Overview of the effect of vibration on heat transfer under forced convection conditions [27]

<i>t</i>	Experimental medium	Diameter [mm ⁻¹]	Amplitude [mm ⁻¹]	Frequency [Hz ⁻¹]	Result
Lemlich	Atmosphere	0.64, 1.00 2.06	1.4-5.87	39-122	<i>h</i> 4-fold increase
Deaver	Water	0.18	2.54-70	4.25	<i>h</i> 4-fold increase
Lemlich	Water and aqueous glycerin	1.25	0.05-2.18	17-37	<i>h</i> 12.28-fold increase
Penny	Water	0.20	63.5	4.5	<i>h</i> 5-fold increase
Penny	Ethylene glycol	0.20	63.5	4.5	<i>h</i> 2.5-fold increase
Hsieh	Water	10.0	0.16-6035	27-51	<i>h</i> 0.54-fold increase
Dawood	Atmosphere	8.5, 12.7	0-17.8	0-68	<i>h</i> 3-fold increase

Table 1 provides an overview of the effect of vibrational heat transfer under forced convection conditions. As table shown, the effect of vibrational heat transfer varies significantly with the flow state of the experimental medium, however, the results reported in the literature are slightly different. For example, in two-phase heat transfer experiments involving water and water vapor, the maximum reduction in surface heat transfer coefficient is, however, for convective heat transfer conditions involving single-phase fluids, the individual experimental results are more consistent, which can enhance heat transfer by 28.7-311%. In general, the effect of vibration on heat transfer will gradually weaken as the Reynolds number increases. In addition, the properties of the fluid medium will affect vibration-enhanced heat transfer. In the experiments, the effect of vibrational heat transfer of water under the same conditions is better than that of aqueous glycerol.

The effect of vibration on the heat transfer of simple mediums such as water and air has been investigated extensively, however, studies regarding the effect of vibration on the heat transfer of hydrocarbon fuels flowing in cooling channels are scarce. Unlike simple mediums, hydrocarbon fuels exhibit significant changes in terms of their physical parameters, such as density, constant pressure specific heat capacity, thermal conductivity, and kinetic viscosity, as the temperature increases. Particularly near the proposed critical temperature (the temperature corresponding to the peak constant pressure specific heat), the thermal physical properties will change more significantly, which results in a unique heat transfer phenome-

non. Based on literature review, only a few studies have analyzed the effect of vibration on the heat transfer of hydrocarbon fuels flowing in cooling channels, particularly in the critical region. In this study, we investigate the effect of vibration on the heat transfer characteristics of cooling channels, with particular focus on the dynamic effect of external vibration on the trans-critical and critical states.

Experimental system and data processing

Experimental system

To investigate the heat exchange process of hydrocarbon fuel flowing in the hot-end channel with or without external vibration, a high temperature, electric, fuel-oil-heating experimental system was established, where RP-3 aviation kerosene was used. The structure of the system is shown in fig. 1. The hydrocarbon fuel flows from the tank through the advection pump, and a 40 μm filter is installed between the tank and pump to prevent the pump from being damaged by obstructed impurities. After the fuel passes through a shut-off valve and insulating device into a mass-flow meter, it flows through the flow meter, where its flow rate is measured, and then into the heating section. A ceramic square tube is used between the ends of the heating section and the exciter to ensure that the heating section vibrates in only one direction. Twenty-six thermocouples are arranged uniformly on the outer wall of the heating section to measure the temperature of the outer wall surface.

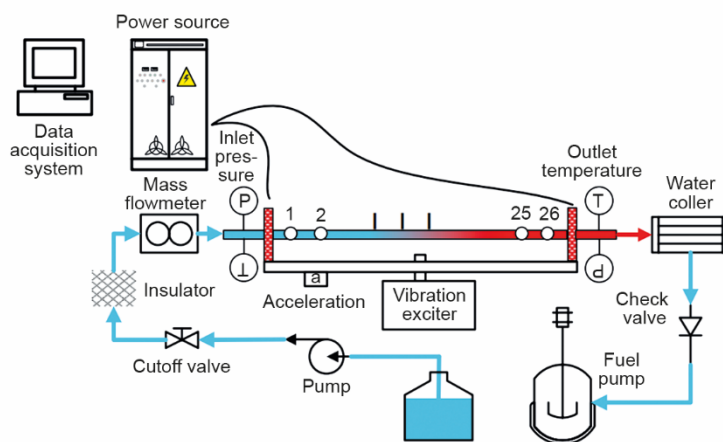


Figure 1. Diagram of experimental system for heat transfer of hydrocarbon fuel flowing at high temperature

The vibration system is switched on when the effect of external vibration on the heat transfer of fuel flowing in the channel is investigated, and switched off when the heat transfer characteristics without external vibration are investigated. After the fuel passes through the experimental tube (or observation section), it enters the cooling recovery system. The experimental equipment comprises the following components: a power supply cabinet powered by a DC regulated power supply with a maximum power of 6 kW, and a plunger pump powered by an SP1020 high pressure infusion pump with a pressure resistance of 25 MPa (Sanotac). An E series CMF010 flow meter from Micro Motion, USA, with a maximum measurable flow rate of 108 kg/h and a pressure resistance of 40 MPa, was used to measure the mass-flow rate. The fluid temperature was measured using a 0.3 mm diameter *K*-type armored thermocouple. To

improve the response to the changing of oil temperature, the head of the armored thermocouple must be grounded off to reduce the heat capacity of the thermocouple. A 10 MPa range pressure transmitter from Shaanxi Microsensor was used to measure the pressure. A data acquisition system from National Instruments, USA was utilized. The exciter used was a DH40100 model from Donghua Test Instruments Co., Ltd., with a maximum excitation force of 100 N and a frequency range of 0.1 Hz to 2.5 kHz. A DH5872 model amplifier from Donghua Test Instruments Co. with a rated output of 200 W and a frequency range of 0-40 kHz DC was used. Additionally, a DH1301 generator from Donghua was used. An acceleration sensor, (Model 1A316E, Donghua Test Instruments Co., Ltd.) with a sensitivity of ~ 5 mV/ms² and a range of 1000 m/s² was used. In terms of the axial vibration, a vibration of approximately 10 Hz can cause the pipe to oscillate, consequently, the heating section is not guaranteed to not move only along the axial direction. Therefore, the heating section was fixed on the guide rail to limit the movement of the heating section in other directions. Meanwhile, the radial vibration did not result in swaying in other directions, hence, a slide rail device need not be used to impose restrictions.

Experimental principle and method

Herein, the heat transfer characteristics refer to the variation in the local heat transfer coefficient or Nusselt number over the entire surface with the oil temperature in the presence or absence of external vibration, and the effects of parameters such as system pressure, heat flow density, flow rate, vibration direction, vibration frequency, and vibration amplitude on the variation. The data acquisition includes direct and indirect measurements. In the experiment, direct measurement is performed via the direct reading of data through the sensor, including parameters such as the flow rate, pressure, inlet oil temperature, voltage, current, outer wall temperature, and vibration acceleration. Meanwhile, indirect measurement is performed for certain physical quantities that are difficult to measure, or for certain variables whose theoretical value cannot be measured and can only be obtained by calculating the directly measured quantities. The method to obtain the heat transfer coefficient and Nusselt number using the directly measured parameters is explained in this section.

The local heat transfer coefficient is:

$$h_x = \frac{q_x}{T_{w,x,in} - T_{b,x}} \quad (1)$$

where q_x is the heat flux on the local wall, $T_{w,x,in}$ the local internal wall temperature, and $T_{b,x}$ the local oil temperature.

The local Nusselt number is:

$$Nu_x = \frac{h_x d_i}{\lambda_x} \quad (2)$$

where d_i is the inner diameter of the experimental tube, and λ_x is the local thermal conductivity of the kerosene. The physical quantities directly measured in the experiment are: the inlet oil temperature of the fuel oil T_{in} , outlet oil temperature T_{out} , inlet flow rate of the fuel oil \dot{m} , 26 outer wall temperatures $T_{w,o,x}$ uniformly arranged in the heating section, outlet pressure, P , of the experimental tube, heating voltage, U , of the experimental tube, and heating current, I . To obtain the heat transfer information, the local heat flux q_x , local inner wall temperature $T_{w,i,x}$, and local oil temperature $T_{b,x}$ must be deduced from these directly measured physical quantities to obtain the local heat transfer coefficient and Nusselt number.

Assuming that the length of the heating section is L and the current flowing through the heating section is I , the local heat flux is:

$$q_x = \frac{I^2 R_x}{\pi d_{in} L} - q_{loss,x} \quad (3)$$

where R_x is the resistance of the control body, d_{in} – the inner diameter of the experimental tube, and $q_{loss,x}$ – the local heat dissipation density. The resistance of the stainless-steel tube R_x is:

$$R_x = \frac{4\rho_x L}{\pi(d_{out}^2 - d_{in}^2)} \quad (4)$$

where ρ_x is the resistivity of the stainless steel and d_{out} is the outer diameter of the experimental tube. Substituting eq. (1) into (2) yields:

$$q_x = \frac{4I^2 \rho_x}{\pi d_{in} (d_{out}^2 - d_{in}^2)} - q_{loss,x} \quad (5)$$

Equation (5) shows the formula for obtaining the local heat flux using known quantities, where the stainless steel resistivity, ρ_x , is a function of the local outer wall temperature $T_{wo,x}$. The local heat dissipation density, $q_{loss,x}$, is associated with the characteristics and size of the heat dissipation surface as well as the temperature difference of the environment, furthermore, it is only a function of the outer wall temperature, $T_{wo,x}$, for a specified experimental tube size and ambient temperature. Both of these functions can be obtained via calibration prior to the experiment. As show in eq. (2), the local heat flux is a function of the current flowing through the experimental tube, inner and outer diameters of the experimental tube, and local outer wall temperature. When measuring the outer wall temperature, the inner wall temperature can be calculated using a 1-D pipe heat transfer equation with an internal heat source.

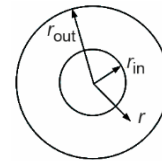


Figure 2. Schematic of local inner wall temperature calculation

The differential equation for thermal conductivity in column coordinates is::

$$\frac{1}{r} \frac{\partial}{\partial r} \left(\lambda_s r \frac{\partial T}{\partial r} \right) + \dot{\Phi} = 0 \quad (6)$$

$$\dot{\Phi} = \frac{I^2 R(T)}{\pi^2 (r_{out}^2 - r_{in}^2)} \quad (7)$$

where λ_s is the thermal conductivity of stainless steel and $\dot{\Phi}$ is the volumetric heat source. The boundary conditions are $T = T_{wo,x}$ for $r = r_{out}$, and $\lambda_s (\partial T / \partial r) = -q_{loss,x}$. Thus, the inner wall temperature can be obtained by integrating from r_{in} to r_{out} , fig. 2, and the inner wall temperature:

$$T_{wx,in} = \frac{\left(T_{wx,out} - \dot{\Phi} \frac{r_{out}^2}{2} - q_{x,loss} r_{out} \right) \ln \frac{r_{out}}{r_{in}} - \frac{\dot{\Phi}}{4} (r_{out}^2 - r_{in}^2)}{k_x} \quad (8)$$

Equation (8) shows the formula for the local inner wall temperature. As shown, the inner wall temperature is determined by the current flowing through the heating section, internal and external diameters of the heating section, local outer wall temperature, and thermal conductivity of stainless steel. Because the pipe of the heating section used in this experiment has a thin wall, the temperature gap inside the tube and on the outer wall is extremely small, and the temperature gradient in the radial direction of the stainless steel is small. Hence, to calculate the thermal conductivity of stainless steel, the thermal conductivity corresponding to the external wall temperature is used.

The ability of the pipe to dissipate heat to the surrounding air can be calibrated using an empty heating experiment. The tube is filled with atmospheric pressure stationary air, subsequently, the heating tube is heated. When the system is in equilibrium, the power delivered to the heating tube by the power supply is equal to that dissipated by the heating tube to the outside air at that time, as convection heat transfer does not occur. At this time, assuming that the effect of axial heat conduction at both ends of the heating tube is limited, the average temperature in the middle section of the heating tube is used. Owing to axial heat conduction, the temperature at the two ends of the heating tube is lower than that at the middle section. Therefore, we assume that the average temperature of the middle section is that of the entire tube. In other words, when no axial heat conduction occurs at both ends, the temperature at both ends of the heating tube is approximately equal to the average temperature. The fitted curve can be expressed in the form of a polynomial function:

$$\dot{q}_{\text{loss}}(T_{\text{wo}}) = \frac{UI}{A_{jh}} = a(T_{\text{wo}} - T_0)^3 + b(T_{\text{wo}} - T_0)^2 + c(T_{\text{wo}} - T_0) + d \quad (9)$$

where $\dot{q}_{\text{loss}}(T_{\text{wo}})$ [Wm^{-2}] is the heat flux density of heat loss in the heating tube T_{wo} [$^{\circ}\text{C}$] – the temperature of the outer wall surface of the tube, A_{jh} [m^2] – the outer surface area of the heating tube used, and T_0 [$^{\circ}\text{C}$] – the ambient temperature. Similar to the inner wall temperature, the fuel temperature inside the heating section cannot be measured directly and can only be approximated. Curve fitting is performed based on the total heat sink of the fuel along the full tube to the oil temperature of the fuel outlet:

$$\dot{Q}_{\text{total}} = f(\bar{T}_{\text{out}}) = a\bar{T}_{\text{out}}^4 + b\bar{T}_{\text{out}}^3 + c\bar{T}_{\text{out}}^2 + d\bar{T}_{\text{out}} + e \quad (10)$$

where \bar{T}_{out} [$^{\circ}\text{C}$] is the outlet oil temperature of the heating section. Because the thermocouple measures the average temperature of the section, it is symbolically represented by the average temperature. Furthermore, the average temperature of the working medium in the tube can be back-calculated using the fitted curve based on the heat sink at a local location:

$$\bar{T}_f = f^{-1}(\dot{Q}_{\text{total}}) \quad (11)$$

Data uncertainty analysis

The heating section has a length of 500 mm, an inner diameter of 2 mm, and a wall thickness of 0.5 mm. The heating section is connected to the electrodes at both ends, and the pipe is heated by adjusting the electrical power at both ends of the electrodes. Thermocouples are evenly welded on the wall of the heating section, each thermocouple being 20 mm apart with a total of 26 thermocouples. Information regarding the heat exchange in the pipe flow is primarily calculated using the 26 thermocouples on the wall of the pipe, inlet and outlet fuel

mainstream temperatures, and inlet and outlet pressures. Therefore, the accuracy of the measured temperature and pressure is crucial.

Table 2. Uncertainty of direct measurement data

Measurement parameters	Installations	Precision
Outer wall temperature, [K]	K-type thermocouple	±0.5K
Oil temperature, [K]	armored thermocouple	±0.5K
Inner diameter, [mm]	scanning electron microscope	±0.0005
Mass-flow rate, [gs ⁻¹]	coriolis mass-flowmeter	±0.15%
Voltage, [V]	voltmeter	±0.2%
Current, [A]	ammeter	±0.2%

The uncertainty of the directly measured experimental data is shown in tab. 2. The uncertainty of the inner wall temperature is 1.05 K for all experimental conditions because the temperature difference between the inner and outer walls is within 2 K:

$$\left| \frac{\delta(\Delta T)}{\Delta T} \right| = \frac{\sqrt{|\delta T_{wx,in}|^2 + |\delta T_{bx}|^2}}{30} = 4.5\% \quad (12)$$

Because the total heat flux and heat loss are two independent variables, the following uncertainties can be derived from the error propagation equation:

$$\left| \frac{\Delta q_x}{q_x} \right| = \sqrt{\left(\frac{q_x + q_{loss}}{q_x} \right)^2 \varepsilon^2(q_{0,x}) + \left(\frac{q_{loss,x}}{q_x} \right)^2 \varepsilon^2(q_{loss,x})} \quad (13)$$

The uncertainty of the total heat flux is:

$$\left| \frac{\Delta q_x}{q_x} \right| = \sqrt{4\varepsilon^2(I) + \left(\frac{2d_{out}^2}{d_{out}^2 - d_{in}^2} \right)^2 \varepsilon^2(d_{out}) + \left(\frac{2d_{in}^2}{d_{out}^2 - d_{in}^2} \right)^2 \varepsilon^2(d_{in}) + \varepsilon^2(d_{out})} = 1.37\% \quad (14)$$

Therefore, the uncertainty of the heat loss is:

$$\left| \frac{\Delta q_{loss,x}}{q_{loss,x}} \right| = \sqrt{\varepsilon^2(U) + \varepsilon^2(I) + \varepsilon^2(d_{out}) + \varepsilon^2(L) + \varepsilon^2(T_{wx,out})} = 0.85\% \quad (15)$$

When the ratio of heat loss to effective heat flux is less than 5%, the value obtained using eqs. (13) is 1.43%. Based on the derivation above, the uncertainty of the heat transfer coefficient can be obtained:

$$\left| \frac{\Delta h_x}{h_x} \right| = \sqrt{\varepsilon^2(q_x) + \varepsilon^2(\Delta T)} = \sqrt{(1.43\%)^2 + (4.5\%)^2} = 4.73\% \quad (16)$$

The previous measurements indicate that the uncertainty in the thermal conductivity of the hydrocarbon fuels is within 3%, and the uncertainty in the internal diameter is 0.46%. Thus, the maximum uncertainty in the Nusselt number can be defined:

$$\left| \frac{\Delta \text{Nu}_x}{\text{Nu}_x} \right| = \sqrt{\varepsilon^2(h_x) + \varepsilon^2(\lambda) + \varepsilon^2(d_{in})} = \sqrt{(4.73\%)^2 + (3.0\%)^2 + (0.46\%)^2} = 5.62\% \quad (17)$$

Result

Subcritical pressure vibration affects gas phase heat transfer

Under a subcritical pressure, hydrocarbon fuel undergoes liquid, gas-liquid, and gas phases successively. Therefore, its heat transfer process can be categorized into three stages: liquid phase, two-phase, and gas phase heat transfer. This section presents an analysis of the flow heat transfer characteristics of hydrocarbon fuel in the hot-end channel under pressures of 0.1 and 2 MPa. When a pressure of 0.1 MPa was set, the heating power was 150 kW/m²K, the flow rate was 1 g/s, and the inlet temperature was 293 K. The variations in the inner wall temperature T_w and the mainstream temperature T_b along the flow direction are shown in figs. 3 and 4, respectively, where x/d represents the dimensionless distance in the flow direction, and the mainstream is classified into four regions A, B, C, and D along the flow direction.

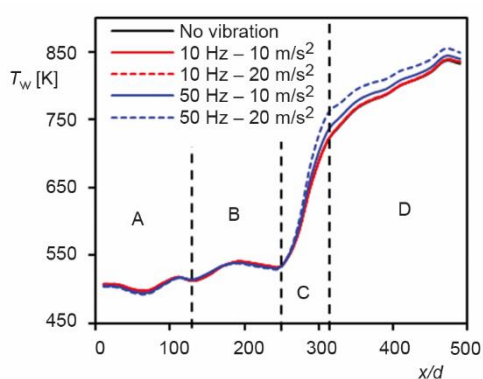


Figure 3. Variation in internal temperature along flow direction

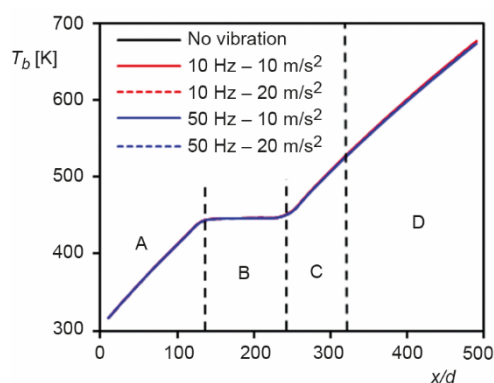


Figure 4. Variation in mainstream temperature along flow direction

In region A or when $x/d < 130$, the outer temperature remains at approximately 500 K, whereas the central fuel flow temperature increased approximately linearly. This occurs because within the thin layer of fluid immediately adjacent to the wall, weak boiling occurs. Subsequently, once the wall is overheated, a new flow began boiling, where heat is absorbed and then dissipated, therefore, the wall temperature remains around the boiling point. This type of weak boiling is different from the typical boiling. When weak boiling occurs, the sub-cooling of the main stream remains high, therefore, the bubbles generated by boiling cool in the main stream and annihilate rapidly, whereas the main stream absorbs heat to increase the temperature gradually. In conventional boiling, the main stream temperature is approximately the boiling point, the bubbles generated by the boiling does not return to liquid phase, and the temperature of the gas-liquid two-phase flow always remains at approximately the boiling point until all the liquid changes into gas. During this phase, axial and radial vibrations barely

affect heat transfer. Figures 5 and 6 show the change in the physical properties along the flow direction, where a linear decrease in density is observed in region A. The decrease is marginal, with the mainstream remaining in the liquid state and a linear increase in the constant pressure specific heat capacity, which consequently result in an increase in the heat transfer coefficient.

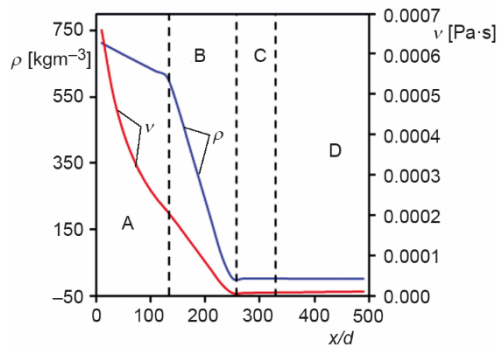


Figure 5. Variation in density and constant-pressure specific heat capacity along flow direction

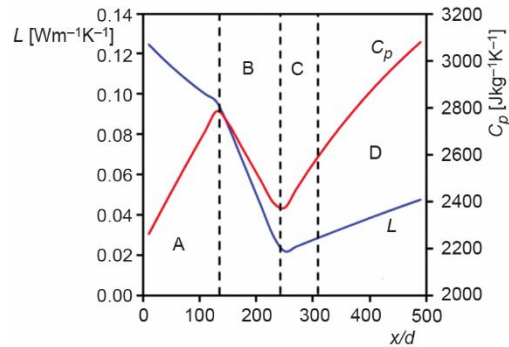


Figure 6. Thermal conductivity and viscosity variation along flow direction

Region B or when $130 < x/d < 250$, shows the distribution of the inner wall temperature and the central flow temperature in the two-phase heat transfer of the hydrocarbon fuel along the tube length. As shown in the figure, the central flow temperature is almost constant, and the wall temperature remains stable at approximately 520 K. The fluid temperature is almost constant near the boiling point, indicating an incomplete vaporization and boiling heat transfer within the experimental tube, instead of a single-phase heat transfer. The abrupt decrease in density indicates nucleate boiling in the tube, and numerous bubbles are generated at the superheated walls and escape into the main stream, which results in a lower heat absorption capacity. Meanwhile, the temperature of the mainstream remains high and approach the boiling point, therefore, the bubbles do not re-condense into liquid but move downward with the liquid mainstream. When nucleate boiling develops to the extent where numerous bubbles accumulate at the wall surface and cover the wall, film boiling occurs, which results in a rapid increase in the wall temperature. At this time, the flow near the wall is in the form of gas, and the thickness of the gas film increases continuously with the tube length, consequently, the thermal resistance increases, which causes the wall temperature to continue increasing. In region C where $250 < x/d < 310$, the liquid film disappears, the density and viscosity decrease to the minimum value and remain stable, and wet steam comes into direct contact with the wall surface. Furthermore, the wall temperature increases significantly. In region D where $x/d > 310$, the working medium enters the dry-steam single-phase heat transfer phase after the wet steam is heated. The density and viscosity remain constant, whereas the thermal conductivity and constant pressure specific heat capacity increase linearly.

Near-critical pressure vibration influences deteriorating heat transfer in transcritical temperature region

A pressure that does not exceed the critical level significantly is known as the near-critical pressure. The settings used in the experiment were: working pressure is 3 MPa, heat-

ing power is $200 \text{ W/m}^2\text{K}$, flow rate is 0.55 g/s , and inlet temperature is 293 K . As 3 MPa is greater than the critical pressure of the hydrocarbon fuel, no boiling occurs, however, a transcritical temperature region emerges at when the physical properties change significantly. Figures 7 and 8 show the variation in the fuel properties in the flow direction. As shown, when $x/d < 270$, the fuel is in the subcritical zone; when $270 < x/d < 380$, the fuel is in the transcritical zone, where the density and constant pressure specific heat capacity change significantly, resulting in heat exchange enhancement; when $x/d > 380$, the fuel is in the supercritical state and the properties change seamlessly.

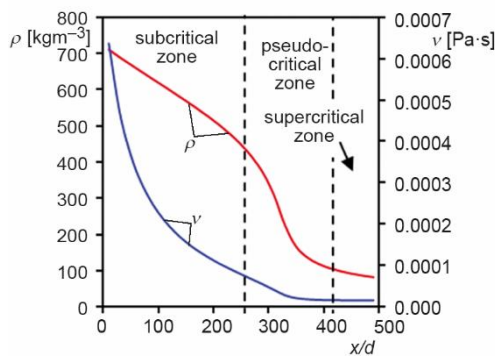


Figure 7. Variation in density and constant-pressure specific heat capacity along flow direction

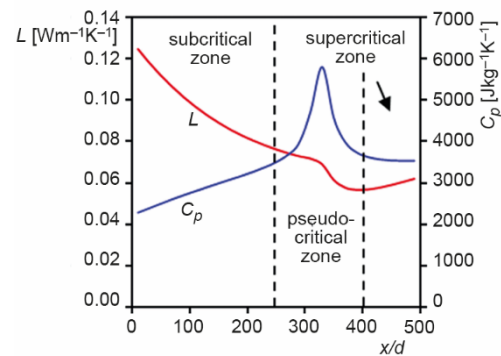


Figure 8. Thermal conductivity and viscosity along flow direction

The variations in the inner wall surface temperature and mainstream temperature along the flow direction are shown in figs. 9 and 10, respectively. As the axial and radial vibrations do not affect the fuel temperature whereas the radial vibration exerts a greater effect on the wall surface temperature than the axial vibration, only the results for the radial vibration are presented herein. As shown in the figures, the wall surface temperature in the transcritical region decreases significantly, without the effect of external vibration. This is because the specific heat at a constant pressure, as shown in fig. 8, reaches its maximum value, and the fuel heat absorption capacity reaches its peak, resulting in an abrupt decrease in the wall sur-

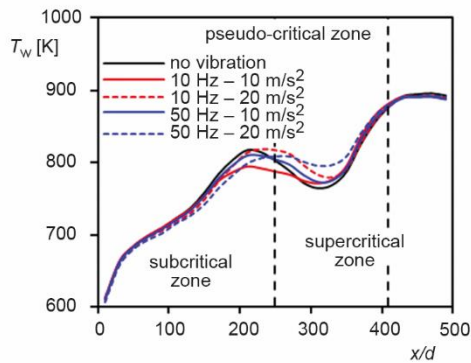


Figure 9. Variation in internal wall temperature along flow direction

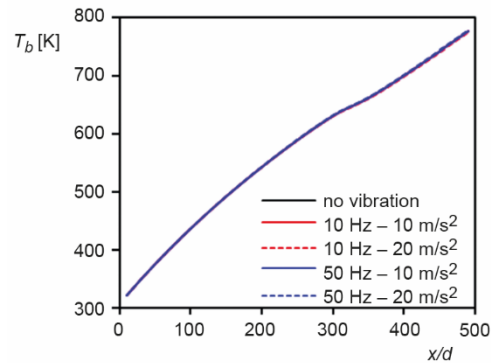


Figure 10. Variation in fuel central flow temperature along flow direction

face temperature. In this region, the heat absorption capacity of the fuel is high, but the physical properties of the fuel change significantly, as such, instability is likely to occur. When external vibration is applied, the wall temperature changes. A vibration of 50 Hz decelerates the decreasing trend of wall temperature.

The effects of axial and longitudinal vibrations on the heat transfer coefficient along the path are shown in figs. 11 and 12, respectively. As shown, the fuel temperature is not affected by the vibration and the wall temperature changes significantly because of the vibration. Therefore, the variation in the heat transfer coefficient is primarily due to the change in the wall temperature. In the absence of vibration, a significant temperature shift in the wall temperature occurs at the laminar turbulent critical position and the constant-pressure specific heat mega position, whereas the radial vibration tends to prevent this shift. An increase in the frequency and acceleration amplitude of vibration results in a smoother temperature shift.

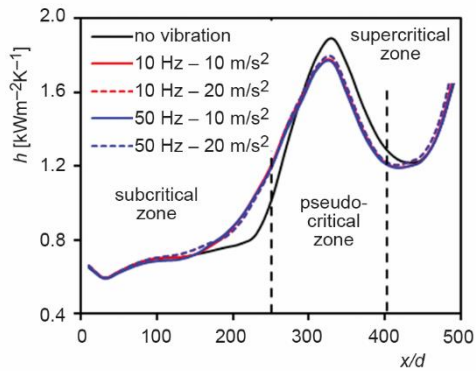


Figure 11. Variation in heat transfer coefficient along range of axial vibration conditions

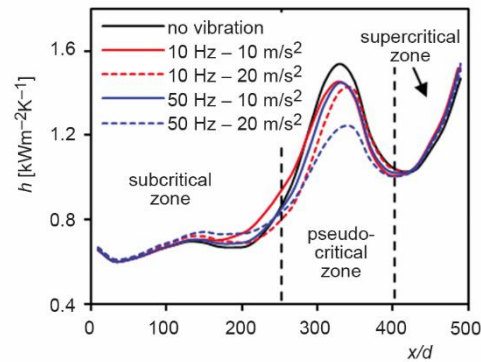


Figure 12. Variation in heat transfer coefficient under radial vibration along the path

Supercritical pressure vibration to enhance heat transfer

To prevent film boiling from occurring in the fuel during cooling, the pressure in the hot-end channel is typically set higher than the supercritical pressure of the fuel. As the temperature increases, the fuel undergoes three thermodynamic states, *i.e.*, subcritical, transcritical and supercritical, throughout the cooling process, and its physical properties change significantly during the process. At the supercritical pressure, the fuel density and specific heat under a constant pressure change the most significantly in the subcritical and transcritical temperature regions. Subsequently, the physical properties change gradually in the supercritical region. This characteristic change in physical properties causes the hydrocarbon fuel to exhibit various flow field properties, including in the region below the supercritical region, where cracking reactions do not occur.

To investigate the effect of external vibration on the heat transfer characteristics of the hot-end channel under the supercritical pressure, we specified the operating conditions as follows: pressure is 4 Mpa, flow rate is 0.55 g/s, and inlet temperature is 293 K. The effect of radial vibration on the heat transfer coefficient along the pipe at heating powers of 70 and 140 W/m²K is shown in figs. 13 and 14, respectively. When the heating power is 70 W/m²K, the effect of external vibration with different frequencies and acceleration amplitudes on the heat transfer coefficient is insignificant. However, when the heating power is 140 W/m²K, the

external vibration imposes a greater effect on the heat transfer coefficient at the back end of the pipe, and the effect of vibration with different frequencies and different amplitudes on the heat transfer coefficient varies. The higher the frequency, the greater is the enhancement in the heat transfer coefficient, meanwhile, the higher the acceleration amplitude, the higher is the acceleration amplitude.

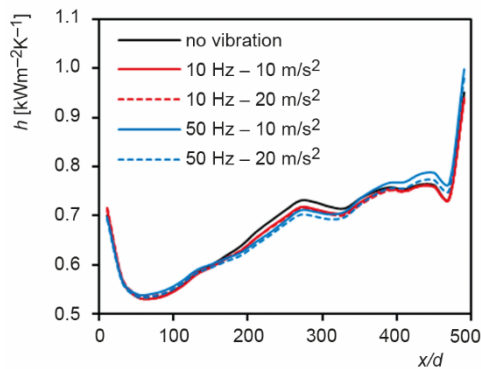


Figure 13. Variation in heat transfer coefficient along the path (70 W/m²K)

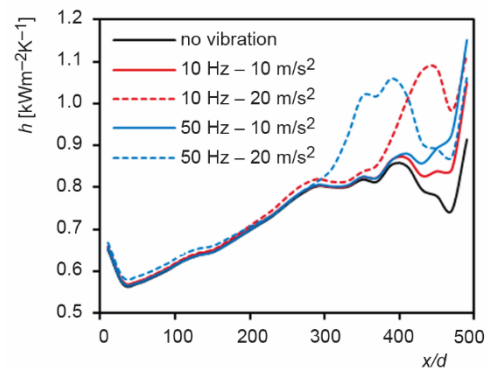


Figure 14. Variation in heat transfer coefficient along the path (140 W/m²K)

Different heating powers under the same external vibration cause different changes to the heat transfer characteristics. Moreover, the increase in the heating power changes the fuel temperature and thus the thermal properties. As shown in figs. 15 and 16, the variations in the mainstream temperature and boundary layer temperature along the flow direction differ for different heat flow densities. The mainstream temperatures along the flow direction under heating powers of 70 W/m²K and 140 W/m²K are less than the proposed critical temperature, and the thermal properties of the mainstream change only slightly. Meanwhile, the fuel temperatures at the boundary layer under heating powers of 70 W/m²K and 140 W/m²K can be approximated using the inner wall temperature, and the results are shown in figs. 15 and 16, respectively. When the heating power is 70 W/m²K, the fuel temperature at the boundary layer remains less than the proposed critical temperature. Similar to the observation in the subcritical state, the change in fuel properties is marginal, therefore, the effect of vibration on the

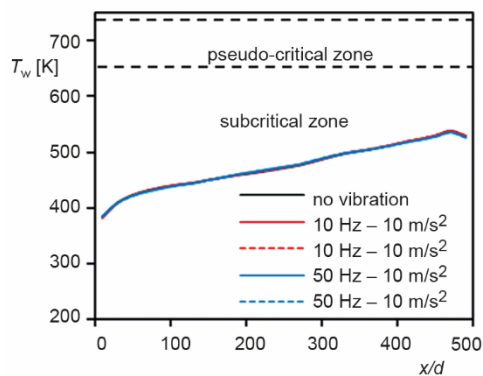


Figure 15. Variation in internal wall temperature along the path (70 KW/m²K)

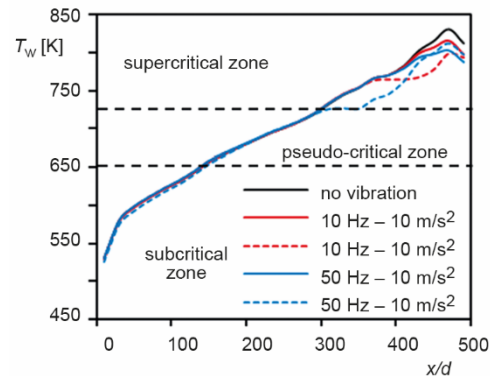


Figure 16. Variation in internal wall temperature along the path (140 KW/m²K)

heat transfer coefficient is insignificant. When the heating power is $140 \text{ W/m}^2\text{K}$, the temperature at the boundary layer undergoes the subcritical, proposed critical, and supercritical states in the flow direction. Furthermore, vibration affects the fuel in the supercritical state, which causes the boundary layer to exhibit a decrease in the wall temperature when the fuel is in the supercritical state; consequently, the heat transfer in this region is enhanced.

The variations in the heat transfer coefficient and temperature of the inner wall surface along the flow direction under a pressure of 5 MPa, flow rate of 1.5 g/s, and heating power of $80 \text{ W/m}^2\text{K}$ are shown in figs. 17 and 18. When the vibration frequency is 10 Hz, the heat transfer is almost unaffected by the vibration. Meanwhile, when the vibration frequency is 50 Hz, the vibration causes an increase in the heat transfer coefficient in the adjacent outlet section. Because the mainstream temperature is below 500 K, which is significantly below the critical temperature, the change in the mainstream thermal properties is insignificant, however, the fuel temperature in the boundary-layer at the outlet section is in the critical region, which is consistent with the heat-transfer-enhanced region arising from vibration. It is inferred that the external vibration of a certain frequency disrupts the fuel in the boundary-layer across the critical state, which may result in a lower wall temperature and heat transfer enhancement.

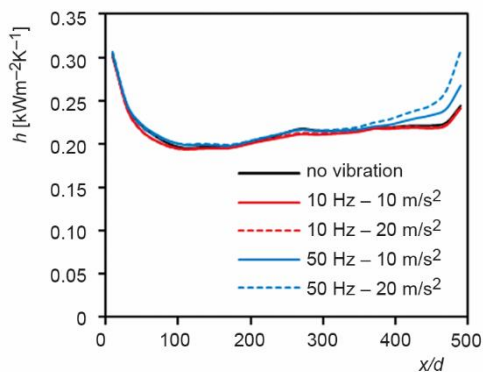


Figure 17. Variation in heat transfer coefficient along the path ($80 \text{ W/m}^2\text{K}$)

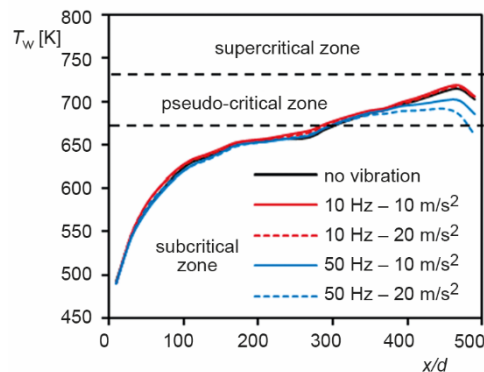


Figure 18. Variation in internal wall temperature along the path ($80 \text{ W/m}^2\text{K}$)

The variations in heat transfer coefficient and internal wall surface temperature along the flow direction under a pressure of 5 MPa, flow rate of 1.5 g/s, and heating power of $120 \text{ W/m}^2\text{K}$ are shown in figs. 19 and 20. Consistent with the findings, the external vibration barely affects the heat transfer when the fuel in the boundary-layer is in the subcritical state, however, when the fuel in the boundary-layer is in the trans-critical and supercritical states, external vibration reduces the wall surface temperature, thereby enhancing heat transfer. Therefore, at the supercritical pressure, external vibration affects heat transfer primarily via the boundary-layer. In fact, it affects the fuel in the boundary-layer only in the trans-critical and supercritical states, and not in the subcritical state.

Effect of external vibration on hot-end channel flow heat transfer

The effect of external vibration on the heat transfer coefficient at subcritical, near-critical, and supercritical pressures is shown in fig. 21. Herein, 0.1 MPa represents the subcritical pressure, 3 MPa the near-critical pressure, and 5 MPa the supercritical pressure.

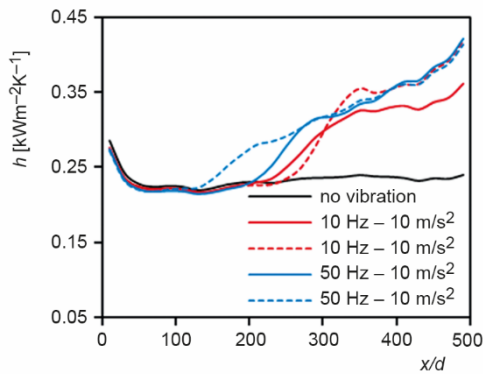


Figure 19. Variation in heat transfer coefficient along the path (120 W/m²K)

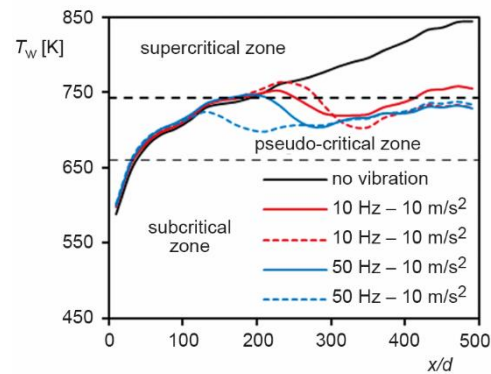


Figure 20. Variation in internal wall temperature along the path (120 W/m²K)

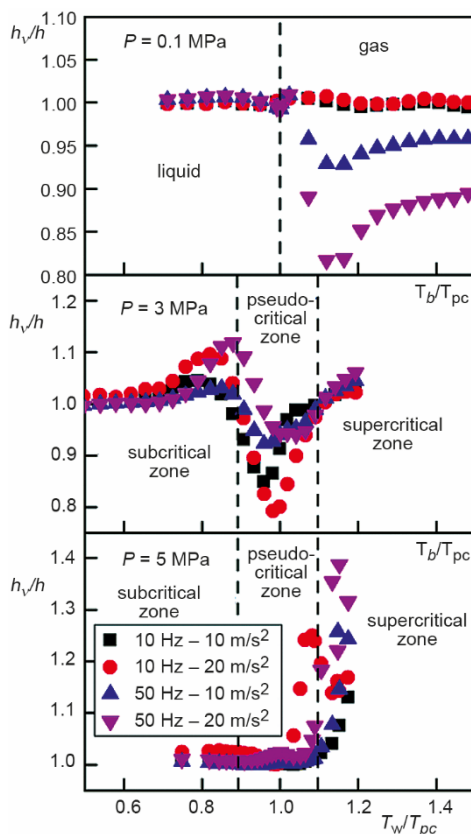


Figure 21. Effect of vibration on flow heat transfer in cooling channel under different pressure conditions

The analysis shows that external vibration barely affects the main flow temperature of the fuel but significantly affects the wall temperature and heat transfer coefficient, indicating that ex-

Under subcritical and near-critical pressures, the horizontal co-ordinate of the graph is the ratio of the mainstream temperature to the critical temperature. Meanwhile, under the supercritical pressure, it represents the ratio of the near-wall fluid temperature to the critical temperature. The vertical co-ordinate represents the ratio of the heat transfer coefficient under vibration to that without vibration, which reflects the effect of vibration on heat transfer in the hot-end channels. Under the subcritical pressure, the fuel is in the liquid state, and heat transfer is unaffected by external vibration. Vibration begins to affect heat transfer only when the fuel passes the phase-change point and becomes gaseous. Under the near-critical pressure, external vibration does not pose a significant effect in the sub-critical temperature range. When the fuel in the tube is in the trans-critical temperature range, its physical properties change significantly, the constant-pressure specific heat capacity reaches its peak, and the heat transfer coefficient increases significantly, whereas external vibration deteriorates heat transfer and weakens the significant change in heat transfer. Under supercritical pressure conditions, external vibration intensifies heat transfer in the hot-end channel only when the oil temperature is below the critical temperature and the internal wall temperature is above the critical pressure.

ternal vibration affects primarily the temperature boundary-layer of the fuel. External vibration causes an additional inertial force on the boundary-layer fluid, which does not affect the boundary-layer heat transfer when the inertial force is relatively small, but affects the heat transfer at the boundary-layer after the inertial force reaches a certain level, the magnitude of which is determined by the vibration frequency and vibration acceleration.

Conclusions

In this study, the effect of vibration on flow heat transfer in cooling channels was investigated experimentally, with particular attention to variations in the trans-critical and supercritical regions. The conclusions are summarized as follows.

- Under the subcritical pressure, external vibration did not affect the heat transfer of liquid-phase fuels. They only exerted an effect when the fuel passed through the phase-change point and became gaseous. The higher the frequency of the vibration, the greater was the effect.
- Under the near-critical pressure, external vibration did not significantly affect the fuel in the subcritical temperature range but can deteriorate the fuel heat transfer across the critical temperature range.
- Under the supercritical pressure, external vibration intensified heat transfer in the hot-end channels only when the fuel temperature was below the critical temperature and the internal wall temperature was above the critical pressure.

References

- [1] Zhang, J. L., et al., Investigations on Flame Liftoff Characteristics in Liquid-kerosene Fueled Supersonic Combustor Equipped with Thin Strut, *Aerospace Science and Technology*, 84 (2019), Jan., pp. 686-697
- [2] Srinivasan, K., et al., Supersonic Combustion of A Scramjet Engine Using Hydrogen Fuel in Shock Tunnel, *AIAA*, 56 (2018), 9, pp. 3600-3609
- [3] Ma, J. C., et al., Control-Oriented Unsteady One-Dimensional Model for A Hydrocarbon Regeneratively-Cooled Scramjet Engine, *Aerospace Science and Technology*, 85 (2019), Feb., pp. 158-170
- [4] Gascoin, N., et al., Validation of Transient Cooling Modeling for Hypersonic Application, *Journal of Thermophysics and Heat Transfer*, 21 (2007), 1, pp. 86-94
- [5] Qin, A., et al., Multi-Objective Optimization on Regenerative Cooling Structure of Scramjet (in Chinese), *Journal of Propulsion Technology*, 39 (2018), 6, pp. 136-144
- [6] Zhang, S. L., et al., Review on Regenerative Cooling Technology of Hypersonic Propulsion (in Chinese), *Journal of Propulsion Technology*, 39 (2018), 10, pp. 23-36
- [7] Han, Y., et al., Assessment of a Hybrid RANS/LES Simulation Method and URANS Method in Depicting the Unsteady Motions of Flow Structures in a Scramjet Combustor, *Aerospace Science and Technology*, 72 (2018), Jan., pp. 114-122
- [8] Ma, F., et al., Thermoacoustic Flow Instability in a Scramjet Combustor, *Proceedings*, 41st AIAA/ASME/SAE/ASEE Joint Propulsion Conference & Exhibit, Tucson, Ariz., USA, 2005: 3824
- [9] Lemlich, Robert., Effect of Vibration on Natural Convective Heat Transfer, *Industrial & Engineering Chemistry*, 47 (1955), 6, pp. 61-73
- [10] Lemlich, R., Rao, M. A., The Effect of Transverse Vibration on Free Convection from a Horizontal Cylinder, *International Journal of Heat & Mass Transfer*, 8 (1965), 1, pp. 27-33
- [11] Deaver, F. K., et al., Heat Transfer From an Oscillating Horizontal Wire to Water, *Journal of Heat Transfer*, 84 (1966), 3, 251
- [12] Penney, W. R., Jefferson, T. B., Heat Transfer From an Oscillating Horizontal Wire to Water and Ethylene Glycol, *Journal of Heat Transfer*, 88 (1966), 4, 359
- [13] Hsieh, R., Marsters, G. F., Heat Transfer from a Vibrating Vertical Array of Horizontal Cylinders, *The Canadian Journal of Chemical Engineering*, 51 (1973), 3, pp. 302-306
- [14] Dawood, A. S., et al., The Effect of Vertical Vibrations on Natural Convection Heat Transfer from a Horizontal Cylinder, *International Journal of Heat & Mass Transfer*, 24 (1981), 3, pp. 491-496

- [15] Scanlan, J. A., Effects of Normal Surface Vibration on Laminar Forced Convective Heat Transfer, *Industrial & Engineering Chemistry*, 50 (1958), 10, pp. 1565-1568
- [16] Saxena, U. C., et al., Heat Transfer from a Cylinder Oscillating in a Cross-Flow, *Journal of Heat Transfer*, 100 (1978), 4, pp. 684-689
- [17] Leung, C. T., et al., Heat Transfer From a Vibrating Cylinder, *Journal of Sound & Vibration*, 75 (1981), 4, pp. 581-582
- [18] Katinas, V. I., et al., Heat Transfer Behavior of Vibrating Tubes Operating in Crossflow. 1. Temperature and Velocity Fluctuations, *Heat Transfer-Soviet Research*, 18 (1986), 2, pp. 1-9
- [19] Cheng, C. H., et al., Experimental Study of the Effect of Transverse Oscillation on Convection Heat Transfer From a Circular Cylinder, *Journal of Heat Transfer*, 119 (1997), 3, pp. 474-482
- [20] Gau, C., et al., Heat Transfer Enhancement and Vortex Flow Structure over a Heated Cylinder Oscillating in the Crossflow Direction, *Journal of Heat Transfer*, 121 (1999), 4, pp. 789-795
- [21] Bronfenbrener, L., et al., Experimental Study of Heat Transfer Intensification under Vibration Condition, *Chemical Engineering & Technology*, 24 (2015), 4, pp. 367-371
- [22] Fu, W. S., Tong, B. H., Numerical Investigation of Heat Transfer from a Heated Oscillating Cylinder in a Cross Flow, *International Journal of Heat & Mass Transfer*, 45 (2002), 14, pp. 3033-3043
- [23] Lee, Y. H., et al., An Experimental Investigation on the Critical Heat Flux Enhancement by Mechanical Vibration in Vertical Round Tube, *Nuclear Engineering & Design*, 229 (2004), 1, pp. 47-58
- [24] Leng, X. L., et al., Heat Transfer Properties of the Vibrational Pipe When Fluid Passes by It Slowly (in Chinese), *Journal of Engineering Thermophysics*, 24 (2003), 2, pp. 328-330
- [25] Klaczak A., Report from Experiments on Heat Transfer by Forced Vibrations of Exchangers, *Heat & Mass Transfer*, 32 (1997), 6, pp. 477-480
- [26] Sarhan, A. R., Karima., et al., Experimental Investigation on the Effect of Vertical Vibration on Thermal Performances of Rectangular Flat Plate (in Chinese), *Experimental Thermal and Fluid Science*, 101 (2019), Jan., pp. 231-240
- [27] Jiang B., Analysis on Mechanism of Heat Transfer Enhancement by Vibration and Experimental Research on a New Type of Vibrational Heat Transfer Component, Ph. D. thesis, Shandong Shandong University, China, 2010